MatP delays the segregation of chromosome termini independently of cell division and tetramer formation in *Vibrio cholerae*

Elena Espinosa[1#], Jihane Challita[1#], Jean-Michel Desfontaines[1], Christophe Possoz[1], Marie-Eve Val[2], Didier Mazel[2], Martial Marbouty[3], Romain Koszul[3], Elisa Galli[1@], and François-Xavier Barre[1@]

[1] Institute for Integrative Biology of the Cell (I2BC), Université Paris-Saclay, CEA, CNRS, Université Paris Sud, 1 Avenue de la Terrasse, 91198 Gif-sur-Yvette, France

[2] Institut Pasteur, Université Paris Cité, CNRS UMR3525, Unité Plasticité du Génome Bactérien, Paris 75015, France

[3] Institut Pasteur, Université Paris Cité, CNRS UMR3525, Unité Spatial Regulation of Genomes, Paris 75015, France

[#] Contributed equally to the work

[@] To whom correspondence should be addressed. Tel: +33 169 823 224; Email: francois-xavier.barre@i2bc.paris-saclay.fr, elisa.galli@i2bc.paris-saclay.fr

Abstract

The cellular arrangement and segregation choreography of the genetic material is involved in the timing of assembly and cellular positioning of the cell division apparatus in bacteria. Key to this mode of regulation is the positioning of sister copies of the replication terminus zone (*ter*) of the chromosomes at the end of the replication cycle. The *Vibrio cholerae* genome is distributed on two chromosomes, ChrI and ChrII. ChrI is derived from the ancestor of the Vibrionales and Enterobacterales. ChrII is derived from a megaplasmid. ChrI encodes for a homologue of MatP, a protein that tethers sister copies of the *ter* of the *Escherichia coli* chromosome together at mid-cell at the time of cell division. MatP structures the *ter* by binding to a *ter*-specific DNA motif, *matS*. It forms tetramers that can bridge DNA segments together and it connects sister *ter* copies to the divisome via an interaction with a cell division protein, ZapB. We find that MatP structures the *ter* of ChrI and ChrII, *ter1* and *ter2*, and ensures the cohesion and mid-cell position of sister *ter1* and *ter2* copies at the time of cell division, demonstrating that ChrII is organised and behaves as a *bona fide* chromosome. We show that cohesion and positioning are independent of cell division and tetramer formation, but are linked to the local density of *matS* sites, with sister *ter2* separating earlier than sister *ter1* because of a lower number of *matS* sites. Overall, our results suggest that the primary mechanism of action of MatP is to slow down the decatenation of newly replicated molecules.

Introduction

Chromosome segregation and cell division must be coordinated in space and time to ensure the faithful transmission of genetic information. In eukaryotes, this is achieved by linking several steps of cytokinesis to the assembly and activity of the mitotic spindle, the eukaryotic chromosome segregation machinery. In bacteria, which lack a functional equivalent of the mitotic spindle, the genomic DNA itself is involved in the regulation of cell division (1–3). This has been remarkably illustrated in *Vibrio cholerae* - the causative agent of the deadly human diarrhoeal disease of the same name, in which positioning and timing of assembly of the cell

division apparatus, the divisome, is primarily dictated by the cellular arrangement and choreography of segregation of the chromosomes (4, 5).

V. cholerae is a curved rod-shaped bacterium with a single polar flagellum (Figure 1A). Its genome is divided in two chromosomes, ChrI and ChrII. Each of these carries a single origin of replication, *ori1* and *ori2*, with replication terminating in a diametrically opposite zone, *ter1* and *ter2*, in which is located a site dedicated to the resolution of chromosome dimers, *dif1* and *dif2,* by the XerCD/FtsK machinery (Figure 1B, (6, 7)). They are longitudinally arranged within the cell, with *ter1* and *ter2* migrating from the pole opposite to the flagellum to mid-cell in the course of the replication/segregation cycle (Figure 1A, (8, 9)). Binding sites for a DNA-associated protein that inhibits FtsZ ring formation, SlmA, are enriched all along ChrI and ChrII except for *ter1* and *ter2* (Figure 1A, (1, 4)). Hence, the longitudinal arrangement and choreography of segregation of ChrI and ChrII sequesters cell division proteins at the new pole of newborn cells and restricts septum formation to the centre of the cell at the end of the replication/segregation cycle (Figure 1A, (4, 5)).

Key to this mode of regulation is the positioning of *ter1* and *ter2*. Accordingly, we observed cell division defects in MCH1, a synthetic mono-chromosomal strain in which all of ChrII except *ori2* and its partition machinery is inserted in ChrI at the *dif1* locus (4). We also noticed that cell division was affected when the homologue of the *E. coli* MatP protein was deleted (4). *E. coli* MatP forms dimers that bind to a DNA motif, *matS*, which is overrepresented within the replication terminus of the *E. coli* chromosome, *ter* (10–12). MatP restricts contacts between *ter* and the rest of the genome (12, 13) and ensures the colocalization of sister *ter* copies at mid-cell (14, 15). The latter action was proposed to be related to the self-interaction of the 20 carboxy terminal amino acids of the protein, leading to the formation of tetramers (dimers of dimers) that bridge sister *matS* sites together after replication (11, 16), and/or to the interaction of the same residues with a cell division protein, ZapB, which tethers *ter* to the FtsZ ring (17–19). Functional homologues of MatP and ZapB similarly connect the terminus zone of the *Caulobacter crescentus* chromosome to the FtsZ ring (14, 15). Together, these observations suggested that MatP was involved in the correct positioning of sister *ter1* and *ter2* copies.

Consistent with this view, multiple copies of the *E. coli matS* motif are present in *ter1* and *ter2* (9, 12), and we previously showed that *V. cholerae* MatP maintained sister copies of *dif1* together at mid-cell until the onset of constriction (9, 20). However, we found that sister copies of *dif2* separated and moved away from mid-cell prior to the onset of constriction (9). In addition, we observed that sister copies of *dif1* remained associated independently of divisome assembly during the recovery of *V. cholerae* spheroplasts to a proliferative rod-shaped state (21).

Here, we investigate how MatP participates to the cellular arrangement and choreography of segregation of the two *V. cholerae* chromosomes by analysing the phenotype and chromosome organisation of wild-type cells, *matP* and cell division mutants using a combination of deep sequencing and fluorescence microscopy techniques. We find that *ter1* and *ter2* both harbour numerous *matS* sites, with a similar but broader motif than the *E. coli matS* consensus. We show that MatP structures both *ter1* and *ter2* into macrodomains and addresses them at mid-cell at the time of cell division, suggesting that ChrII behaves as a *bona fide* chromosome from an organisational and functional point. We demonstrate that MatP-mediated cohesion and cellular positioning is independent of cell division and tetramer formation, but is linked to the local density of *matS* sites, with sister *ter2* separating earlier than sister *ter1* because of a lower number of *matS* sites. Overall, our results suggest that the primary mechanism of action of MatP is to slow down the decatenation of newly replicated molecules.

Results

Numerous *matS* sites flank both *dif1* and *dif2*

We previously noticed that a conserved amino acid motif differentiated the Vibrionales and Enterobacterales MatP proteins (22). This raised the possibility that *V. cholerae* MatP bound to a different DNA motif than *E. coli* MatP, which would be over- and under-represented in *ter1* and *ter2*, respectively (9). To check this possibility, we used ChIP-seq to explore the binding of a functional FLAG version of *V. cholerae* MatP on ChrI and ChrII *in vivo*.

ChIP-seq revealed 44 and 34 MatP-bound sites on ChrI and ChrII, respectively (Figure 1C and Table S1). Searching for sites that could fit with the MEME motif using MCAST revealed 17 and 5 additional potential sites for the binding of MatP on ChrI and ChrII, respectively (Table S2, (23)). These sites were not enriched in the ChIP-seq data, suggesting that a factor prevented the binding of MatP at their locations *in vivo* (Figure S1A). Bioinformatic analysis using MEME showed that the sites bound by *V. cholerae* MatP corresponded to a 13 bp motif similar to but broader than the *E. coli matS* motif (Figure S1B, (12, 24)). No significant difference was observed in the sequence logos of the MatP-bound sites harboured by ChrI and ChrII (Figure 1C).

Several lines of evidence suggest that all of the different *V. cholerae* MatP binding sites we identified are functional *matS* sites. First, *V. cholerae* MatP binding sites that deviated from the *E. coli matS* consensus were not less enriched than sites that followed the *E. coli matS* consensus. For instance, the site with the lowest similarity score to the *V. cholerae* MatP consensus corresponded to the highest peak in the ChIP-seq profile of N16961 *V. cholerae* cells (Figure 1C and Table S1). Second, sites harbouring the exact same DNA motif showed different ChIP-seq enrichments (Table S2 and Figure S1A). Third, most of the MatP-binding sites were located in the terminal proximal part of the chromosomes (Figure 1C, Table S1 and S2). A notable exception was a site close to *ori2*. However, we previously noticed that *ter1* harboured a very strong SlmA binding site (SBS) and a binding site for ParAB2 (*parS2*) separated by only 68 bp, which suggested that a translocation event occurred between the *ori2* region and *ter1* (4, 25).

The MatP domain of the *E. coli* chromosome was defined as the longest stretch of DNA containing *matS* sites that was flanked by 100 kbp regions devoid of *matS* sites (12). Based on the same criteria, 41 out of the 44 *matS* sites of ChrI defined a 587 kbp MatP domain centred on *dif1*, and 33 out of the 34 *matS* sites of ChrII defined a 537 kbp MatP domain centred on *dif2* (Figure 1C and Table S1). Within these domains, the most highly enriched *matS* sites tended to be those closest to *dif1* and *dif2* (Figure 1C). This was not explained by any *matS* sequence specificity (Table S1), but was correlated with the local density of *matS*

sites (Figure S1C). Indeed, the increase in the density of *matS* sites in the vicinity of *dif1* and *dif2* explained by itself the enrichment of MatP-bound sequences at *dif1* and *dif2* (Figure S1D).

MatP acts on both *ter1* and *ter2*

The ChrI and ChrII MatP domains have a mean density of 7 and 6 *matS* sites per 100 kbp. This is over twice higher than the density of *matS* sites in the *E. coli* MatP domain (12). It raised the possibility that the differential management of *ter1* and *ter2* was due to a factor specifically preventing the action of MatP on ChrII. To check this possibility, we analysed whether *V. cholerae* MatP was able to insulate the ChrI and ChrII MatP domains from flanking chromosomal regions, as observed for *E. coli* MatP (10, 12, 13). To this end, we applied 3C coupled with deep sequencing to exponentially growing WT and Δ*matP* N16961 cells. As previously reported, the contact map showed that each of the 2 chromosomes displayed a single strong diagonal resulting from the enrichment of contacts between adjacent loci (Figure S1E, (26)). The width of the main diagonal of the contact map was smaller in the ChrI and ChrII MatP domains than in the rest of the genome, reflecting a reduction of long-range *cis* contacts (Figure S1E, (26)). The absence of a secondary diagonal perpendicular to the main one, further suggested a lack of *cis* contacts between the replication arms of each chromosome (Figure S1E, (26)). ChrI-ChrII contacts formed a cross in the *trans* contact part of the 3C-seq map. The centre of the cross indicated contacts between *ter1* and *ter2*. The arms of the cross corresponded to contacts along the whole length of the ChrII replication arms and the terminal half of the ChrI replication arms (Figure S1E, (26)). Deletion of *matP* profoundly altered chromosome contacts (Figure S1F). To highlight the changes, we plotted the ratio of Δ*matP* and WT contact signals (Figure 1D). In the absence of MatP, we observed an enrichment of *cis* contacts within the MatP domains and between the MatP domains and their flanking regions (Figure 1D). This led to frequent contacts between *ori2* and *ter2*, suggesting that ChrII had entirely lost its structural conformation (Figure 1D). The increase in *cis* contacts was accompanied by a decrease in contacts between ChrI and ChrII (Figure 1D).

MatP has a minor role in the positioning of ChrII loci

As 3C-seq demonstrated that MatP was able to act on both ChrI and ChrII, we decided to investigate in detail its role in the cellular arrangement and segregation choreography of ChrI and ChrII. To this end, we analysed the cellular position of 12 genomic loci in snapshot images. These included loci in the immediate vicinity of *ori1*, *ori2*, *dif1* and *dif2* (OI, OII, DI and DII), 4 loci within the MatP domain of ChrI (L5I, L6I, R6I and R5I), 2 loci on the right replication arm of ChrI (R2I and R4I), and one locus on each of the two replication arms of ChrII (L2II and R3II) (Figure 1B).

We generated a series of 11 *matP*$^+$ and 11 Δ*matP* strains in which OI was tagged with the ParB^{pMT1}-YGFP/*parS*^{pMT1} labelling system and one of each of the other 11 loci was tagged with the mCherry-LacI/*lacO* fluorescent repressor/operator array labelling system (8, 27, 28). Slow growth conditions were used to ensure a single replication/segregation cycle per division. Thus, each labelled locus gave rise to one or two spots, depending on whether replication had reached its chromosomal location and sister copies were separated or not. It permitted to orient cells on the basis that the OI labelled locus is located at the old pole (the pole inherited form the mother cell) of newborn cells and that one of its replicated copies remained at the old pole during the replication/segregation (8). We separately analysed the position of each locus in cells in which it gave rise to a single spot or two spots, hereafter referred to as 1-spot and 2-spots cells (Table S3). In 1-spot *matP*$^+$ cells, the longitudinal axis position of each ChrI and ChrII labelled locus increased almost linearly as a function of its genomic distance from DI and DII, respectively (Figure 2A, top panel). DI was very close to the new pole, i.e. the pole resulting from the mother cell division (Figure 2A, top panel). DII was located in the newer half of the cell pole, at approximately the same longitudinal position as R4I (Figure 2A, top panel). In contrast, in 1-spot Δ*matP* cells, all labelled loci except OI, R2I and OII were located at approximately the same relative distance from the new pole (Figure 2A, top panel). The same trend was observed in 2-spots *matP*$^+$ and Δ*matP* cells (Figure S2A).

Plotting the median distance between separated sister spots further highlighted the altered location of sister copies of the different tagged loci in Δ*matP* cells (Figure 2A, bottom panel). This type of analysis is advantageous because it can be performed without cell orientation,

which allowed us to increase the number of analysed cells for each locus by using strains in which OI was not tagged (Table S3). In *matP*$^{+}$ cells, DI, L5I, L6I, R6I, R5II and R4I sister spots were closer than expected from a linear decrease as a function of their genomic distance from OI (Figure 2A, bottom panel). Although DII sister spots were more distant from each other than DI sister spots, they were closer than expected from a linear decrease as a function of their genomic distance from OII. In Δ*matP* cells, however, distances between sister spots of all loci except OI, R2I and OII were in the same range (Figure 2A, bottom panel).

Taken together, these results showed that MatP influenced the position of loci within a large 1 Mbp zone extending outside of the MatP domain on ChrI and influenced loci situated within a narrow 0.3 Mbp zone inside the MatP domain on ChrII (Figure 2A). The role played by MatP was critical for the position of *ter1* loci and more limited for the position of ChrII loci (Figure 2A).

MatP is involved in *dif1*- and *dif2*-cohesion at the onset of division

Previous marker frequency analysis experiments showed that the number of replicated copies of the ChrI and ChrII loci decreased exponentially as a function of the genomic distance separating them from *ori1* and *ori2*, respectively (6). In contrast, the spot duplication frequencies of OI and R2I were similar (Figure 2B, Top panel). This is probably linked to high cohesiveness of the *ori1* region (29). However, spot duplication frequencies dropped abruptly after R4I, suggesting an increase in cohesion (Figure 2B, top panel). In addition, the spot duplication frequency of DII was lower than expected from a linear decrease as a function of its distance from OII (Figure 2B, top panel). Deletion of *matP* completely suppressed the increased cohesion of the DII locus and reduced cohesion at DI, R6I, L6I, R5I and L5I (Figure 2B, top panel). In addition, the spot duplication frequency now linearly decreased from R2I, R4I, R5I, R6I to DI, as expected from their timing of replication. Correspondingly, deletion of *matP* resulted in a greater increase in the frequency of cells with two spots at loci in the immediate vicinity of *dif1* and *dif2* (grey bars in the upper panel of Figure 2B). These observations suggested that MatP increased the cohesion persistence period within the ChrI and ChrII MatP domains.

To further investigate the role of MatP in sister chromatid cohesion, we used Hi-SC2, a high-throughput, high-resolution whole-genome method for monitoring sister chromatid contacts (29, 30). Hi-SC2 uses paired-end sequencing to determine the status and position of site-specific recombination cassettes that have been randomly-inserted by transposition. The cassettes are composed of two directly repeated recombination sites separated by a DNA segment that is too short to allow their excision by intramolecular recombination. However, intermolecular recombination events between sister copies of a cassette can lead to the formation of a copy with a single recombination site. Therefore, the excision frequency of the cassette, f, can be used as a proxy of the length of time during which sister copies remain in contact. The local frequency of sister chromatid contacts behind replication forks can be monitored using cassettes based on the Cre/*loxP* site-specific recombination system, whose activity is independent of the cell cycle (30–32). The local frequency of sister chromatid contacts after the onset of constriction can be monitored using cassettes based on the XerCD/*dif1* site-specific recombination system, whose activity depends on a direct contact with a cell division protein, FtsK (7, 9, 29). In *matP*$^+$ strains, the excision frequency of short *loxP* cassettes (f_{loxP}) was dramatically higher in the MatP domains than in the rest of the genome (Figure 2B, middle panel (29)). The excision frequency of short *dif1* cassettes (f_{dif1}) was null at all genomic positions except in the immediate vicinity of *dif1* and *dif2* (Figure 2B, bottom panel (29)). FtsK is a DNA translocase (33, 34). FtsK oriented polar sequences (KOPS) pointing towards *dif1* and *dif2* direct its translocation, which could affect the possibility for *dif1* recombination (7, 35, 36). However, a large *dif1* cassette, which allows intra-molecular recombination, was excised at a frequency greater than 50% in a third of ChrI and half of ChrII, indicating that *dif1* recombination was not restricted to the immediate proximity of *dif1* and *dif2* (Figure S2B). f_{loxP} was similar at *dif1* and *dif2* (Figure 2B, middle panel), but f_{dif1} was considerably lower at *dif2* than at *dif1* (Figure 2B, bottom panel). Taken together, these results suggested that cohesion was higher in the MatP domains than in the rest of the genome and that sister copies of loci remained in contact during constriction in the immediate vicinity of *dif1*

and, in a much more limited extent, *dif2*, in agreement with the sister spot duplication observations.

Deletion of *matP* didn't modify f_{loxP} in ChrI except in the MatP domain where 44% of the sister chromatid contacts were lost (Figure 2B, middle panel). It increased f_{loxP} in the replication arms of ChrII except in a 150 kbp zone within the MatP domain where 23% of the sister chromatid contacts were lost (Figure 2B, middle panel). However, only a third and a half of f_{dif1} was retained in the immediate vicinity of *dif1* and *dif2*, respectively (Figure 2B, bottom panel). Taken together, these results showed that MatP played a minor but significant role in the post-replicative cohesion of loci within the ChrI and ChrII MatP domains, and a major role in the persistence of cohesion in the immediate vicinity of *dif1* and *dif2* at the time of cell division. Yet, deletion of *matP* didn't fully alleviate the low sister spot duplication and high post-replicative cohesion of loci within the MatP domains, and the increased frequency of sister chromatid contacts in the vicinity of *dif1* and *dif2* during constriction.

MatP prolongs sister chromatid contacts between consecutive MatP domains

To gain further insight into the role of MatP in the arrangement and segregation of chromosomes, we analysed its action in MCH1, in which ChrII is integrated into the MatP domain of ChrI (Figure 3A (37)). Previous work showed that replication of the MCH1 chromosome starts at *ori1* and ends in *ter2* (4), and that chromosome dimers are efficiently resolved by the addition of crossovers at *dif2* (37).

ChIP-seq experiments using the FLAG version of *V. cholerae* MatP showed that the binding pattern of MatP in the *ter2* zone of the MCH1 chromosome was similar to that of N16961 ChrII (Figure 3B, S1D, S3A and Table S4). The insertion of ChrII into *dif1* splits the ChrI MatP domain into two halves, which are located on opposite replication arms at 0.5 Mbp from *dif2* (Figure 3B). The binding pattern of MatP in the two halves of the ChrI MatP domain was similar in MCH1 and N16961 (Figure 3B, S1D, S3A and Table S4). Thus, there are 3 MatP domains in MCH1: one in the *ter2* zone, one in the right replichore and one in the left replichore. The most highly enriched sequences were located at the centre of the *ter2* MatP domain (Figure 3B, note that the highly enriched *matS* site located near *ori2* in N16861 is absent from the

MCH1 chromosome). The most highly enriched *matS* sites in the right replichore MatP domain were comparable to those of the *ter2* MatP domain (Figure 3B). However, the most highly enriched *matS* sites in the left replichore MatP domain were twice lower than those of the *ter2* MatP domain (Figure 3B and S3A).

We analysed the arrangement of the MCH1 chromosome by labelling 11 loci (Figure 3A). These included the OI, OII and DII loci, 5 loci on the right replication arm (R1I, R3I, R5I, OII and L1II) and 4 loci on the left replication arm (R3II, R1II, L6I and L5I) of the chromosome (Table S3). In 1-spot *matP*$^+$ MCH1 cells, the long axis distance between the spot of each labelled locus and the new pole increased almost linearly as a function of their genomic distance from DII (Figure 3C, top panel). Sister spots of R5I and OII were slightly closer to the new pole than expected (Figure 3C, bottom panel). DII was closer to the new pole than it was in 1-spot N16961 cells, but further away from it than DI in 1-spot N16961 cells (Figure 1C and 3C, top panel). The same trend was observed for the distance between sister spots (Figure 3C, bottom panel) and the distance of sister spots from the centre of the cell (Figure S3B). Deletion of *matP* slightly increased the new pole distance of loci comprised between OII and L6I in 1-spot cells (Figure 3C, top panel) and DII was now at the same distance from the new pole than it was in N16961 Δ*matP* cells (Figure 1C and 3C, top panel). The same trend was observed for the distance between sister spots (Figure 3C, bottom panel) and the distance of sister spots from the centre of the cell (Figure S3B). These results suggested that MatP only had a minor, yet significant, role on the arrangement of the MCH1 chromosome.

However, the spot duplication frequency of loci comprised between R5I and L6I was lower than the linear decrease expected based on their replication timing, suggesting that cohesion was increased at these positions (Figure 3D, top panel). Strikingly, deletion of *matP* not only suppressed the increase in cohesion at the DII locus (Figure 3D, top panel), but also reduced cohesion at OII, L6I, R1II, R3II, R5I and L5I (Figure 3D, top panel). Correspondingly, the deletion of *matP* led to a greater increase in the frequency of cells with two spots at these loci (grey bars in the top panel of Figure 3D). In addition, f_{loxP} was high within *ter2*, the right half of *ter1*, and all the intermediate positions between these two zones (Figure 3D, middle panel,

(29)). Deletion of *matP* slightly increased f_{loxP} in the regions corresponding to ChrI but led to a 24% reduction in sister chromatid contacts in the 150 kbp zone surrounding *dif2* (Figure 3D, middle panel). Finally, f_{dif1} was as high at the junction of ChrII with the right replication arm of ChrI as it was at DII, and remained highly elevated in the 800 kbp zone comprised between these loci (Figure 3D, bottom panel). Deletion of *matP* resulted in the loss of 76% of the sister chromatid contacts in this zone at the time of cell division. These results indicated that MatP was able to maintain together sister copies of loci between the *ter2* and the right replichore MatP domains of the MCH1 chromosome, but failed to maintain together sister copies of loci in the left replichore MatP domain.

MatP action depends on the number and local density of *matS* sites

The number and density of *matS* sites in the MatP domain of the left replichore of the MCH1 chromosome is lower than that in the MatP domain of the right replichore, which suggested that a threshold had to be reached for the effect of MatP on cohesion to be visible (Figure 3B). To test this hypothesis, we engineered JVV024, a strain in which two *matS* sites adjacent to *dif1* were displaced next to *dif2* (Figure 4A). It decreased the density of *matS* sites in the ChrI MatP domain from 7 to 6.6 sites per 100 kbp, and increased the density of *matS* sites in the ChrII MatP domain from 6 to 6.4 sites per 100 kbp (Table S5), which mitigated the difference in the enrichment of MatP at DI and DII (Figure 4B). Shifting the two *matS* sites was sufficient to increase f_{dif1} at the DII locus to half of the frequency measured at the DI locus (Figure 4C). It also alleviated the difference in the proportion of cells showing a single DII spot and two DI spots and that of cells showing a single DI spot and two DII spots (Figure 4D, left and middle panels). Correspondingly, the number of cells showing two DI and two DII spots increased (Figure 4D, right panel). Finally, the distance separating DI sister copies was significantly increased in contrast to that separating DII sister copies (Figure 4E).

These results suggested that MatP influenced cohesion at the time of cell division at positions where it was highly enriched, namely *dif1* and *dif2* in N16961 (Figure S1D) and *dif2* and the junction of ChrII with the right replication arm of ChrI in MCH1 (Figure S3A). To test this hypothesis, we constructed a strain in which the right part of the ChrI MatP domain was

inverted, EPV487 (Figure 4F). The inversion created a cleft in the MatP ChIP-seq profile at *dif1* (Figure 4G and Table S6). The position with the highest MatP enrichment was now at the junction of the inverted fragment and the right replication arm (Figure 4G). The f_{dif1} profile followed the local enrichment of MatP (Figure 4H). As with N16961 and MCH1, the high f_{dif1} was mainly associated with MatP (Figure S4A). The proportion of cells showing two DI spots and a single DII spot was higher than that of cells showing a single DI spot and two DII spots, reflecting the decrease in cohesiveness of the DI sister copies in EPV487 (Figure 4D, left and middle panels). Correspondingly, there was an increase in the number of cells with two DI and two DII spots (Figure 4D, right panel). Finally, the inversion significantly affected the distance between DI and DII sister copies (Figure 4E) and the relative timing of duplication of the DI and DII loci (Figure S4B).

Taken together, these results suggested that the effect of MatP on chromosome positioning depended on the number and local density of *matS* sites.

MatP acts independently of cell division

A plasmid with two *matS* sites accumulates at mid-cell in a MatP dependent manner in *E. coli* (17). The localisation pattern of the plasmid was shown to be due to the formation of a proteinaceous bridge between the extreme C-terminus of MatP, ZapB, ZapA and FtsZ (17, 18). In *V. cholerae*, DI localised at mid-cell at the time of cell division, consistent with the idea that MatP coordinated chromosome segregation and cell division by tethering MatP domains to the divisome (Figure 2, (9)). However, DII did not localise at mid-cell at the time of division even though it was flanked by 34 *matS* sites on which the action of MatP was detected, which contradicted this view (Figure 1C and 2, (9)). Therefore, we decided to explore the role of the extreme C-terminus of MatP, ZapB and ZapA in the positioning of DI and DII. To this end, we followed the choreography of segregation of DI by time-lapse video microscopy (Figure 5A and S5A). Results in WT and Δ*matP* N16961 cells recapitulated those of Figure 2. In the presence of MatP, DI localised at the new pole of newborn cells and migrated to mid-cell at the very end of the cell cycle (Figure 5A). Sister DI copies remained associated until the very end of the cell cycle (Figure 5A) and at short distance from each other (Figure 5B). In contrast, in Δ*matP* cells,

DI was randomly distributed between the new pole and mid-cell at birth and the ¼-¾ part of the cell at the end of the cell cycle (Figure 5A and S5A). In addition, sister DI copies separated prior to cell division (Figure S5A) with a distance of over a quarter of the cell length (Figure 5B). Deletion of *matP* also increased the distance between sister DII copies to over a quarter of the cell length (Figure 5B). However, we further noticed that the positioning of OI was slightly affected by the deletion of *matP* (Figure S5B and S5C). Taken together, these results highlighted the role of MatP in the choreography of ChrI segregation.

Based on the homology of *V. cholerae* and *E. coli* MatP, we constructed a C-terminal truncation allele to prevent the formation of MatP dimers, *matP* Δdimer, and an allele truncated from the extreme C-terminus to prevent the formation of MatP tetramers, *matP* Δtetra. The alleles were introduced in place of the WT *matP* allele of N16961. ChIP-seq showed no binding of MatP Δdimer to *matS* sites, as expected from the absence of dimer formation. Correspondingly, cells carrying the *matP* Δdimer allele had the same phenotype as Δ*matP* cells (Figure 5A and 5B). On the contrary, MatP Δtetra had the same binding profile as WT MatP (Figure S5D), the choreography of DI segregation in *matP* Δtetra cells was similar to that of WT cells (Figure 5A) and the distance between DI sister copies was only slightly elevated (Figure 5B). The choreography of DI segregation in Δ*zapA* and Δ*zapB* cells was similar to that of WT cells (Figure 5A) and the distance between DI sister copies was only slightly elevated (Figure 5B). The above results indicated that MatP was able to maintain sister DI copies at mid-cell independently of ZapB and ZapA.

To rule out the possibility that another cell division protein was involved in the cellular distribution of MaP, we compared the choreography of DI segregation in *matP*$^{+}$ and Δ*matP* cells carrying a thermosensitive allele of *ftsZ*, *ftsZ84*^{ts}. Growth of *ftsZ84*^{ts} strains at the non-permissive temperature (42°C) prevents the formation of the FtsZ ring, which leads to the dispersal of the other cell division proteins in the cytoplasm of the cell and filamentation (5). The binding profile of MatP on the genome of *ftsZ84*^{ts} cells grown at 42°C was identical to the binding profile of MatP on the genome of WT N16961cells and *ftsZ84*^{ts} cells grown at the permissive temperature (30°C) (Figure S5D). However, DI copies separated from each other

380 at a much later stage in the *ftsZ84*^{ts} strain grown at 42°C than in its Δ*matP* derivative (Figure
381 5C). Together, these results suggest that MatP kept sister *dif1* sites together at mid-cell
382 independently of the cell division machinery.

383 ## Discussion

384 **MatP structures both *ter1* and *ter2* into macrodomains**

385 ChIP-seq results suggested the existence of a 587 kbp MatP domain centred on *dif1* and a
386 537 kbp MatP domain centred on *dif2* (Figure 1 and Table S1). The 3C-seq contact map
387 showed a low frequency of long-range contacts *in cis* within these domains, indicating that they
388 were constrained (Figure S1). In addition, we observed no long-range contacts *in cis* between
389 the MatP domains and their flanking regions, indicating that they were isolated from the rest of
390 the chromosome on which they were located (Figure S1). However, the 3C-seq contact map
391 revealed frequent contacts *in trans* between *ter1* and *ter2*, which reflected their spatial cellular
392 proximity all along the cell cycle (Figure S1 and Figure 2, (8, 9)). In the absence of MatP, long-
393 range *cis* contacts between each of the MatP domains and their flanking regions appeared
394 (Figure 1). This was particularly dramatic for ChrII, in which any chromosomal locus now
395 contacted any other chromosomal locus (Figure 1). These results demonstrate that *V. cholerae*
396 MatP organises *ter1* and *ter2* into macrodomains that are isolated from the rest of the genome
397 within the cell. It was proposed in *E. coli* that a DNA condesin, MukBEF, favoured long-range
398 *cis* contacts by extruding ~800 kbp intrachromosomal loops all along the chromosome but in
399 *ter*, from which it was excluded and/or inactivated by a direct interaction with MatP (12, 13, 38,
400 39). Future work will need to investigate the interplay between MatP and the homologue of
401 MukBEF in *V. cholerae*.

402 **MatP is involved in the choreography of segregation of *ter1* and *ter2***

403 Deletion of *matP* led to the suppression of *trans* contacts between *ter1* and *ter2*, demonstrating
404 its importance for the coordination of ChrII segregation with that of ChrI (Figure 1).
405 Correspondingly, we found that MatP drove the new pole to mid-cell re-positioning of loci within
406 the ChrI MatP domain and *dif2* in the course of replication (Figure 2 and 5). We further found

that MatP was involved in the cohesion period of sister copies of the ChrI and ChrII MatP domains behind the replication forks (Figure 2 and 3). However, the deletion of *matP* did not entirely suppressed cohesion behind replication forks, suggesting the existence of another cohesion factor. In contrast, MatP was the main factor keeping together at mid-cell sister copies of *dif1* and *dif2* until the onset of division (Figure 2, 3 and 5).

Cohesion and cellular positioning depend on the number and density of *matS* sites

The reduction of long-range *cis* contacts was as important at the border of the ChrI and ChrII MatP domains as in their central part, indicating that a few *matS* sites were sufficient for MatP to organise chromosomal DNA in *V. cholerae*, as previously reported in *E. coli* (Figure 1, (12)). In contrast, the distance separating loci within the ChrI MatP domain from the new pole at the beginning of the cell cycle and the distance separating sister copies of these loci from mid-cell and from each other at the end of the cell cycle increased as a function of their genomic distance from *dif1*, the ChrI locus where the density of *matS* sites is the highest (Figure 1 and 2). In addition, the frequency of sister chromatid contacts behind replication forks correlated with the local density of *matS* sites in the ChrI domain in N16961 (Figure 2), in the right moiety of the ChrI MatP domain when displaced ~500 kbp from the terminus position (Figure 3), or when 150 kb of the domain were inverted (Figure 4). The ChrI MatP domain contains 41 *matS* sites whereas the ChrII MatP domain contains 33 *matS* sites, further suggesting that differences in the cohesion and cellular positioning of sister *dif1* and *dif2* copies at the onset of constriction were linked to the number of *matS* within these domains (Figure 2 and 5). Consistently with this view, the right moiety of the ChrI MatP domain, which harbours 26 *matS* sites, was highly cohesive whereas the left moiety, which harbours 12 *matS* sites, was not (Figure 3). In addition, differences in the cohesion of sister copies of *dif1* and *dif2* loci were alleviated by reducing the number of *matS* sites in the ChrI MatP domain from 41 to 39 and increasing that of the ChrII MatP domain from 33 to 35 (Figure 4). Taken together, these results suggested that the efficiency of MatP-mediated positioning and cohesion of the ChrI and ChrII MatP domains depended on the number and local density of *matS* sites they harboured, and was independent of their timing of replication and their management by FtsK. The presence of

a *matS* site in a phage satellite that is integrated in two copies next to *dif1* (TLCΦ), in several cassettes of the super-integron, which is located next to *dif2*, and in the coding sequence of genes, attests of a selection pressure to maintain the number and local density of *matS* sites in *ter1* and *ter2* (Figure 1 and Table S1). In this regard, we are intrigued by the possibility that the extra-numerous *matS* sites of the ChrI and ChrII MatP domains that were not bound by MatP could serve as backups in conditions impeding the binding of MatP to some of the *matS* sites that were chipped in our study (Table S2).

MatP-mediated positioning is independent of cell division and tetramer formation

The precise mid-cell positioning of *dif1* at the end of the replication cycle and the proximity of sister *dif1* copies after their separation were not altered in Δ*zapA* and Δ*zapB* cells (Figure 5). Likewise, recent high throughput timelapse observations showed that the duration of *ter* mid-cell localisation was barely modified in Δ*zapB* cells in *E. coli* (16). In the present study, we further demonstrate that mid-cell positioning is independent of any other divisome component by showing that MatP delayed the separation of sister *dif1* copies in *ftsZ*^{ts} cells grown at the non-permissive temperature (Figure 5).

MatP tetramers have also been proposed to bridge sister *matS* sites together (11, 16). However, deletion of the tetramerization domain of MatP barely altered the mid-cell positioning of *dif1* and the distance of separation of sister *dif1* copies, ruling out this idea in *V. cholerae* (Figure 5). Correspondingly, *matS* pairing was not detected in contact maps and in *in vitro* assays in *E. coli* (13, 19).

Instead, our results fit with a role of MatP in the regulation of decatenation. Because of the helical nature of double stranded DNA, (+) supercoils accumulate ahead of replication forks. Torsional tension induces the replication machinery to swivel around itself, generating right-handed interlinks that maintain sister chromatids together behind replication forks. Precatenanes and catenation links are removed by the decatenase topoisomerase IV (Topo IV). The correlation between the local density of *matS* sites and the extent of cohesion in the ChrI and ChrII MatP domains behind replication forks suggest that MatP slows down decatenation at the sites where it is bound (Figure 2 and 3). Analysis of the cohesion at the

time of cell division likewise suggests that the speed of decatenation is slower at the sites where the density of *matS* sites is higher, i.e. in the immediate vicinity of *dif1* and *dif2* in N16961, *dif2* and the left side of the right ChrI MatP domain moiety in MCH1 (Figure 3), and a position between R6I and R4I in EPV487 (Figure 4). Finally, decatenation should be faster in *ter2* than in *ter1* because of its lower number and lower density of *matS* sites, leading to the earlier separation of and larger distance between sister copies of *dif2* than sister copies of *dif1* (Figure 4). The small length of ChrII could help decrease the chances to leave unresolved catenation links behind replication forks and/or a tug of war between the ParAB2/*parS*2 and MatP/*matS* systems could help separate sister *ter2* copies. Consistently with this view, sister *ter2* copies separated later in MCH1 than in N16961 (Figure 3). However, sister *ter2* copies still separated earlier in MCH1 than sister *ter1* copies in N16961, indicating that the small size of ChrII and the ParAB2/*parS*2 system played a very minor role in cohesion compared to the number and density of *matS* sites (Figure 2 and 3).

Decatenation should be more effective in *E. coli* than in *V. cholerae* because of the lower number and density of *matS* sites in *ter* than in *ter1* or *ter2*, which could explain the importance of the MatP-ZapB-ZapA-FtsZ connection for the positioning of sister *ter* copies at mid-cell at the time of cell division (17, 19). The presence of a few remaining catenation links could explain why sister *ter* copies separate but remain in close proximity to mid-cell in *E. coli* Δ*zapA*, Δ*zapB* and *matP*Δ20 mutants (11, 16). Consistent with this view, we previously observed that sister *dif2* copies kept colliding against each other at mid-cell after their initial separation in the cell cycle (9).

The regulation of decatenation by MatP is probably linked to the exclusion and/or inactivation of MukBEF, which was shown to recruit and stimulate Topo IV in *E. coli* (40, 41). MukBEF trails behind replication forks in *E. coli* (12). FtsK, which translocates in the same direction as replication, was proposed to remove MatP from *matS* sites (35, 36, 42). However, cohesion at the time of cell division dropped between the left side of the right ChrI MatP domain moiety and *dif2* in MCH1 (Figure 3). In addition, cohesion dropped at *dif1* in EPV487, in which the inversion of the right moiety of the ChrI MatP domain led to a higher density of *matS* sites on

both sides of *dif2* (Figure 4). These observations suggest that MukBEF can load on chromosomes independently of replication even in between MatP-covered regions, as previously suggested in *E. coli* (12). Future work will need to investigate the influence of MukBEF on the formation of precatenanes in the course of replication. Another challenge will be to develop a methodology to directly monitor the catenation links that remain to be removed at the end of the replication/cycle in *E. coli* and *V. cholerae*.

ChrII behaves as a *bona fide* bacterial chromosome from a functional point of view

ChrI is derived from the chromosome of the monochromosomal ancestor of the Vibrionales and Enterobacterales, whereas ChrII is derived from a megaplasmid (43). From a genomic point of view, ChrII is considered as a 'chromosome-plasmid', or chromid, because it carries essential core genes, has a nucleotide composition close to that of ChrI, but possesses plasmid-type replication and partition systems (44). However, we previously showed that ChrII participates to the regulation of the cell cycle because its origin proximal part is enriched in SlmA-binding sites (4). Our ChiP-seq, 3C-seq, fluorescence microscopy and Hi-SC2 results further demonstrate that MatP organises *ter2* into a macrodomain, coordinates its migration with that of *ter1* and ensures its positioning close to mid-cell at the time of cell division, which is essential for the control of cell division by SlmA-mediated nucleoid occlusion (Figure 1, 2, 5). In this regard, ChrII is organised and behaves as a *bona fide* bacterial chromosome. It will be interesting to check whether such a functional definition applies to other chromids.

Methods

Strains, plasmids and oligonucleotides

Bacterial strains, plasmids and oligonucleotides used in this study are listed in Table S7. All strains are derivatives of an El Tor N16961 strain that was rendered competent by the insertion of *hapR* by specific transposition. They were constructed by natural transformation or conjugation with integration/excision plasmids. Strains construction is described in detail in File S1. Engineered strains were confirmed by PCR. Chromosomal loci were visualized by inserting

at selected loci a *parS*^{pMT1} motif or a *lacO* array specifically detected by YGFP-ParB^{pMT1} and LacI-RFPT, respectively.

Microscopy

Cells were grown in M9 minimal medium supplemented with 0.2% fructose and 1 µg/ml thiamine to exponential phase and spread on a 1% (w/v) agar pad (ultrapure agarose, Invitrogen) for analysis. For snapshot analyses, cell images were acquired using a DM6000-B (Leica) microscope and were analysed using MicrobeTracker (45). Table S3 list the number of cells analysed for each chromosomal locus. For time-lapse analyses, the slides were incubated at 30°C or 42°C for *ftsZ*^{ts} analyses and images acquired using an Evolve 512 EMCCD camera (Roper Scientific) attached to an Axio Observe spinning disk (Zeiss). At each time point, we took a stack of 32 bright-field images covering positions 1.6 µm below and above the focal plane. Cell contours were detected and cell genealogies were retraced with a MatLab-based script developed in the lab (4). After the first division event, the new pole and old pole of cells could be unambiguously attributed based on the previous division events.

Hi-SC2

Hi-SC2 transposon libraries were prepared as previously described (29, 30). Briefly, transposons harbouring *loxP* or *dif1* cassettes and a kanamycin resistance gene were introduced in strains conditionally expressing Cre or XerC, respectively. Tight control of the recombinase production was achieved by placing their genes under an arabinose promoter and an antisense β-galactosidase promoter. After overnight growth on LB plates containing kanamycin and IPTG, ~400.000 colonies were scraped, mixed in LB with IPTG and stored in aliquots at -80°C. Aliquots of the transposon library were thawed on ice and ~10^9 cells were diluted into 100 mL of media supplemented with IPTG. Cells were grown until exponential phase (OD_{600} 0.2). Then, ~10^9 cells were centrifuged and transferred into 10 mL of fresh media without IPTG. After 30 minutes, arabinose was added at a final concentration of 0.02%. ~10^9 cells were recovered and frozen in liquid nitrogen after 4 hours of induction for *dif1* cassettes and 90' for *loxP* cassettes. Hi-SC2 libraries were prepared and subjected to pair-end sequencing on a NextSeq 500 (Illumina). After sequencing, barcodes, adapters and

transposon sequence were removed using Cutadapt (46) and files with total reads and reads in which the reporter cassette had excised were created. Finally, the BWA software was used for the alignment of reads on genomes (47) and stored in the SAM format (48).

ChIP-seq

~10^9 cells from overnight cultures harbouring a functional *matP*-FLAG3x allele at the *matP* native locus were diluted into 100 mL of fresh media and were grown until exponential phase (OD_{600} 0.2). Cells were crosslinked for 30' with formaldehyde 37% up to a final concentration of 1%. Crosslinking reactions were quenched for 15' with Glycine 2.5 M up to a final concentration of 250 mM. Samples were centrifuged, washed with TBS (Tris-HCl pH 4.7 50 mM, NaCl 1M) and harvested by centrifugation. After, cells were lysed for 30' at 37°C with 500 µL of lysis buffer I (sucrose 20%, Tris-HCl pH 8 10 mM, NaCl 50 mM, EDTA 10 mM and Lysozyme 1mg/mL (w/v)). Then, 500 µL of lysis buffer II (Tris-HCl pH 4.7 50 mM, NaCl 150 mM, EDTA 1mM, Triton X100 1%, Roche Antiprotease Cocktail) was added and samples were sonicated for 30' (Covaris, Duty cycle 5, Intensity 4, Cycle/burst 200). After sonication, samples were centrifuged at 13000 rpm for 30' at 4°C. Supernatants were collected into a fresh tube, 50 µL were separated to use as control (input). For immunoprecipitation (IP), an Anti-FLAG M2 affinity gel (Sigma) was added to the cell extracts and the volume was adjusted up to 1 mL in lysis buffer II. After an overnight incubation at 4°C on a rotating wheel, samples were centrifuged at 6000 rpm for 30 seconds at 4°C. Pellets were washed twice with TBS mixed with Tween 20 0.05% and three times with TBS. A 3xFLAG elution solution was prepared in buffer (Tris-HCl pH 4.7 500 mM, NaCl 1M) at a concentration of 25 µg/µL and diluted in TBS to a final concentration of 150 ng/µL. 2.5 volumes of elution solution were added per volume of IP sample and input. Samples were incubated for 30' at 4°C on a rotating wheel. Then, samples were eluted twice by centrifugation at 6000 rpm for 30 seconds at 4°C. RNase A was added to a final concentration of 1 µg/mL and samples were incubated for 1 hour at 37°C. Finally, samples were de-crosslinked by the addition of 5 µL of proteinase K (20 mg/ml) and overnight incubation at 65°C. gDNA form input and IP was extracted using a Qiagen PCR Purification Kit and Qiagen MinElute PCR Purification Kit, respectively. Illumina libraries were

prepared using DNA SMART^{TM} ChIP-Seq Kit (TAKARA) following manufacture's protocol. Purified libraries were subjected to sequencing on a NextSeq 500 (Illumina).

Generation of 3C libraries

3C libraries were generated as described (26). In brief, cultures were crosslinked with formaldehyde (3%). Fixed cells were lysed with SDS (0.5%) in the presence of lysozyme (35 U/ml; Tebu Bio). Their genome was subjected to HpaII digestion and re-ligation. The DNA was then purified and quantified on gel using QuantityOne software (BioRad). The resulting 3C library was sheared using a Covaris S220 instrument (Duty cycle 5, Intensity 5, cycles/burst 200, time 60 s for 4 cycles) and sheared DNA fragments were ligated to custom-made MM76 and MM77 adapters (Table S7,(49)). Paired-end sequencing was performed on an Illumina sequencer according to the manufacturer instructions (PairedEnd DNA sample Prep Kit – Illumina – PE-930-1001). The custom-made adapters were removed from the reads using cut-adapt. Data were then analysed using HiC-Pro (50). Visualization of contact-maps and computation of their ratio was performed as described in (13).

ACKNOWLEDGEMENTS

The work was supported by the Agence Nationale pour la Recherche [2018-CE12-0012-03 and 2023-CE12-0018-01 to F.-X.B., 2019-CE35-0013-01 to E.G.] and the Fondation pour la Recherche Médicale [EQU202003010328 to F.-X.B.]. We thank E. Paly for helping in constructing strains and plasmids, V. Lioy, S. Duigou, and Y. Yamaichi for technical advice and helpful discussions.

CONFLICT OF INTEREST

The authors declare no conflict of interest.

REFERENCES

1. Bernhardt,T.G. and de Boer,P.A. (2005) SlmA, a nucleoid-associated, FtsZ binding protein required for blocking septal ring assembly over Chromosomes in E. coli. *Mol Cell*, **18**, 555–64.

2. Thanbichler,M. and Shapiro,L. (2006) MipZ, a spatial regulator coordinating chromosome segregation with cell division in Caulobacter. *Cell*, **126**, 147–162.

3. Wu,L.J. and Errington,J. (2004) Coordination of cell division and chromosome segregation by a nucleoid occlusion protein in Bacillus subtilis. *Cell*, **117**, 915–25.

4. Galli,E., Poidevin,M., Le Bars,R., Desfontaines,J.-M., Muresan,L., Paly,E., Yamaichi,Y. and Barre,F.-X. (2016) Cell division licensing in the multi-chromosomal Vibrio cholerae bacterium. *Nat. Microbiol.*, **1**, 16094.

5. Galli,E., Paly,E. and Barre,F.-X. (2017) Late assembly of the Vibrio cholerae cell division machinery postpones septation to the last 10% of the cell cycle. *Sci. Rep.*, **7**.

6. Galli,E., Ferat,J.-L., Desfontaines,J.-M., Val,M.-E., Skovgaard,O., Barre,F.-X. and Possoz,C. (2019) Replication termination without a replication fork trap. *Sci. Rep.*, **9**, 8315.

7. Val,M.-E., Kennedy,S.P., El Karoui,M., Bonné,L., Chevalier,F. and Barre,F.-X. (2008) FtsK-dependent dimer resolution on multiple chromosomes in the pathogen Vibrio cholerae. *PLoS Genet.*, **4**, e1000201.

8. David,A., Demarre,G., Muresan,L., Paly,E., Barre,F.-X. and Possoz,C. (2014) The two Cis-acting sites, parS1 and oriC1, contribute to the longitudinal organisation of Vibrio cholerae chromosome I. *PLoS Genet.*, **10**, e1004448.

9. Demarre,G., Galli,E., Muresan,L., Paly,E., David,A., Possoz,C. and Barre,F.-X. (2014) Differential management of the replication terminus regions of the two Vibrio cholerae chromosomes during cell division. *PLoS Genet.*, **10**, e1004557.

10. Mercier,R., Petit,M.-A., Schbath,S., Robin,S., El Karoui,M., Boccard,F. and Espéli,O. (2008) The MatP/matS site-specific system organizes the terminus region of the E. coli chromosome into a macrodomain. *Cell*, **135**, 475–485.

11. Dupaigne,P., Tonthat,N.K., Espéli,O., Whitfill,T., Boccard,F. and Schumacher,M.A. (2012) Molecular basis for a protein-mediated DNA-bridging mechanism that functions in condensation of the E. coli chromosome. *Mol. Cell*, **48**, 560–571.

12. Seba,M., Boccard,F. and Duigou,S. Activity of MukBEF for chromosome management in E. coli and its inhibition by MatP. *eLife*, **in press**.

13. Lioy,V.S., Cournac,A., Marbouty,M., Duigou,S., Mozziconacci,J., Espéli,O., Boccard,F. and Koszul,R. (2018) Multiscale Structuring of the E. coli Chromosome by Nucleoid-Associated and Condensin Proteins. *Cell*, **172**, 771-783.e18.

14. Ozaki,S., Wakasugi,Y. and Katayama,T. (2021) Z-Ring-Associated Proteins Regulate Clustering of the Replication Terminus-Binding Protein ZapT in Caulobacter crescentus. *mBio*, **12**, 10.1128/mbio.02196-20.

15. Ozaki,S., Jenal,U. and Katayama,T. (2020) Novel Divisome-Associated Protein Spatially Coupling the Z-Ring with the Chromosomal Replication Terminus in Caulobacter crescentus. *mBio*, **11**, e00487-20.

16. Sadhir,I. and Murray,S.M. (2023) Mid-cell migration of the chromosomal terminus is coupled to origin segregation in Escherichia coli. *Nat. Commun.*, **14**, 7489.

17. Espeli,O., Borne,R., Dupaigne,P., Thiel,A., Gigant,E., Mercier,R. and Boccard,F. (2012) A MatP-divisome interaction coordinates chromosome segregation with cell division in E. coli. *EMBO J.*, **31**, 3198–3211.

18. Galli,E. and Gerdes,K. (2012) FtsZ-ZapA-ZapB interactome of Escherichia coli. *J. Bacteriol.*, **194**, 292–302.

19. Crozat,E., Tardin,C., Salhi,M., Rousseau,P., Lablaine,A., Bertoni,T., Holcman,D., Sclavi,B., Cicuta,P. and Cornet,F. (2020) Post-replicative pairing of sister ter regions in Escherichia coli involves multiple activities of MatP. *Nat. Commun.*, **11**, 3796.

20. Galli,E., Midonet,C., Paly,E. and Barre,F.-X. (2017) Fast growth conditions uncouple the final stages of chromosome segregation and cell division in Escherichia coli. *PLoS Genet.*, **13**, e1006702.

21. Goudin,A., Ferat,J.-L., Possoz,C., Barre,F.-X. and Galli,E. (2023) Recovery of Vibrio cholerae polarized cellular organization after exit from a non-proliferating spheroplast state. *PloS One*, **18**, e0293276.

22. Adam,Y., Brezellec,P., Espinosa,E., Besombes,A., Naquin,D., Paly,E., Possoz,C., van Dijk,E., Barre,F.-X. and Ferat,J.-L. (2022) Plesiomonas shigelloides, an Atypical Enterobacterales with a Vibrio-Related Secondary Chromosome. *Genome Biol. Evol.*, **14**, evac011.

23. Bailey,T.L. and Noble,W.S. (2003) Searching for statistically significant regulatory modules. *Bioinforma. Oxf. Engl.*, **19 Suppl 2**, ii16-25.

24. Bailey,T.L., Boden,M., Buske,F.A., Frith,M., Grant,C.E., Clementi,L., Ren,J., Li,W.W. and Noble,W.S. (2009) MEME SUITE: tools for motif discovery and searching. *Nucleic Acids Res.*, **37**, W202-208.

25. Yamaichi,Y., Fogel,M.A., McLeod,S.M., Hui,M.P. and Waldor,M.K. (2007) Distinct Centromere-Like parS Sites on the Two Chromosomes of Vibrio spp. *J. Bacteriol.*, **189**, 5314–5324.

26. Val,M.-E., Marbouty,M., de Lemos Martins,F., Kennedy,S.P., Kemble,H., Bland,M.J., Possoz,C., Koszul,R., Skovgaard,O. and Mazel,D. (2016) A checkpoint control orchestrates the replication of the two chromosomes of Vibrio cholerae. *Sci. Adv.*, **2**, e1501914–e1501914.

27. Lau,I.F., Filipe,S.R., Søballe,B., Økstad,O.-A., Barre,F.-X. and Sherratt,D.J. (2003) Spatial and temporal organization of replicating Escherichia coli chromosomes. *Mol. Microbiol.*, **49**, 731–743.

28. Nielsen,H.J., Ottesen,J.R., Youngren,B., Austin,S.J. and Hansen,F.G. (2006) The Escherichia coli chromosome is organized with the left and right chromosome arms in separate cell halves. *Mol. Microbiol.*, **62**, 331–338.

29. Espinosa,E., Paly,E. and Barre,F.-X. (2020) High-Resolution Whole-Genome Analysis of Sister-Chromatid Contacts. *Mol. Cell*, **79**, 857-869.e3.

30. Espinosa,E., Yamaichi,Y. and Barre,F.-X. (2020) Protocol for High-Throughput Analysis of Sister-Chromatids Contacts. *STAR Protoc.*, **1**, 100202.

31. Sternberg,N. and Hamilton,D. (1981) Bacteriophage P1 site-specific recombination: I. Recombination between loxP sites. *J. Mol. Biol.*, **150**, 467–486.

32. Abremski,K., Hoess,R. and Sternberg,N. (1983) Studies on the properties of P1 site-specific recombination: evidence for topologically unlinked products following recombination. *Cell*, **32**, 1301–11.

33. Aussel,L., Barre,F.X., Aroyo,M., Stasiak,A., Stasiak,A.Z. and Sherratt,D. (2002) FtsK Is a DNA motor protein that activates chromosome dimer resolution by switching the catalytic state of the XerC and XerD recombinases. *Cell*, **108**, 195–205.

34. Saleh,O.A., Pérals,C., Barre,F.-X. and Allemand,J.-F. (2004) Fast, DNA-sequence independent translocation by FtsK in a single-molecule experiment. *EMBO J.*, **23**, 2430–2439.

35. Bigot,S., Saleh,O.A., Cornet,F., Allemand,J.-F. and Barre,F.-X. (2006) Oriented loading of FtsK on KOPS. *Nat. Struct. Mol. Biol.*, **13**, 1026–1028.

36. Bigot,S., Saleh,O.A., Lesterlin,C., Pages,C., El Karoui,M., Dennis,C., Grigoriev,M., Allemand,J.-F., Barre,F.-X. and Cornet,F. (2005) KOPS: DNA motifs that control E. coli chromosome segregation by orienting the FtsK translocase. *EMBO J.*, **24**, 3770–3780.

37. Val,M.-E., Skovgaard,O., Ducos-Galand,M., Bland,M.J. and Mazel,D. (2012) Genome Engineering in Vibrio cholerae: A Feasible Approach to Address Biological Issues. *PLoS Genet.*, **8**.

38. Nolivos,S. and Sherratt,D. (2014) The bacterial chromosome: architecture and action of bacterial SMC and SMC-like complexes. *FEMS Microbiol. Rev.*, **38**, 380–392.

39. Bürmann,F., Lee,B.-G., Than,T., Sinn,L., O'Reilly,F.J., Yatskevich,S., Rappsilber,J., Hu,B., Nasmyth,K. and Löwe,J. (2019) A folded conformation of MukBEF and cohesin. *Nat. Struct. Mol. Biol.*, **26**, 227–236.

40. Hayama,R. and Marians,K.J. (2010) Physical and functional interaction between the condensin MukB and the decatenase topoisomerase IV in Escherichia coli. *Proc. Natl. Acad. Sci. U. S. A.*, **107**, 18826–18831.

41. Li,Y., Stewart,N.K., Berger,A.J., Vos,S., Schoeffler,A.J., Berger,J.M., Chait,B.T. and Oakley,M.G. (2010) Escherichia coli condensin MukB stimulates topoisomerase IV activity by a direct physical interaction. *Proc. Natl. Acad. Sci. U. S. A.*, **107**, 18832–18837.

42. Stouf,M., Meile,J.-C. and Cornet,F. (2013) FtsK actively segregates sister chromosomes in Escherichia coli. *Proc. Natl. Acad. Sci. U. S. A.*, **110**, 11157–11162.

43. Adams,D.W., Wu,L.J. and Errington,J. (2014) Cell cycle regulation by the bacterial nucleoid. *Curr. Opin. Microbiol.*, **22**, 94–101.

44. Harrison,P.W., Lower,R.P.J., Kim,N.K.D. and Young,J.P.W. (2010) Introducing the bacterial 'chromid': not a chromosome, not a plasmid. *Trends Microbiol.*, **18**, 141–148.

45. Sliusarenko,O., Heinritz,J., Emonet,T. and Jacobs-Wagner,C. (2011) High-throughput, subpixel precision analysis of bacterial morphogenesis and intracellular spatio-temporal dynamics. *Mol. Microbiol.*, **80**, 612–627.

46. Martin,M. (2011) Cutadapt removes adapter sequences from high-throughput sequencing reads. *EMBnet.journal*, **17**, 10–12.

47. Li,H. and Durbin,R. (2010) Fast and accurate long-read alignment with Burrows–Wheeler transform. *Bioinformatics*, **26**, 589–595.

48. Li,H., Handsaker,B., Wysoker,A., Fennell,T., Ruan,J., Homer,N., Marth,G., Abecasis,G. and Durbin,R. (2009) The Sequence Alignment/Map format and SAMtools. *Bioinformatics*, **25**, 2078–2079.

49. Marbouty,M., Cournac,A., Flot,J.-F., Marie-Nelly,H., Mozziconacci,J. and Koszul,R. (2014) Metagenomic chromosome conformation capture (meta3C) unveils the diversity of chromosome organization in microorganisms. *eLife*, **3**.

50. Servant,N., Varoquaux,N., Lajoie,B.R., Viara,E., Chen,C.-J., Vert,J.-P., Heard,E., Dekker,J. and Barillot,E. (2015) HiC-Pro: an optimized and flexible pipeline for Hi-C data processing. *Genome Biol.*, **16**, 259.

FIGURE LEGENDS

Figure 1. MatP creates a macrodomain in the *ter1* and *ter2* chromosomal zones.

(A) Schematic of newborn and ready to divide *V. cholerae* cells. Spiral line: flagellum; grey shading: cell division proteins; blue and green gradients: SlmA-mediated nucleoid occlusion gradient. By convention, the longitudinal axis coordinates of the new pole and the old pole are set to 0 and 1, respectively. **(B)** *V. cholerae* chromosome maps. ChrI and ChrII are depicted in blue and green, respectively. Black disks: *ori1* and *ori2*; white disks: *dif1* and *dif2*; black rectangles: super integron (SI), Vibrio Pathogenicity Islands (VPI1, VPI2), Vibrio Seventh pandemic Islands (VSP1, VSP2) and O-antigene cluster (Oanti), as indicated. The position of *crtS* and of the loci tagged for microscopic observation are indicated. **(C)** ChIP-seq analysis of the binding of *V. cholerae* MatP. Blue and green lines: relative sequence enrichment profiles along ChrI and ChrII, respectively. The profiles were smoothed using a sliding average distance of 100 bp and scaled between 0 (lowest enrichment locus along the whole genome) and 1 (highest enrichment locus over the whole genome, indicated with a star). The MEME logo of the *matS* sites found on ChrI and ChrII is shown above their respective profiles. There were no significant differences between the position wright matrix of the ChrI and ChrII sites (p-value: 8.44E-11, q-value:1.69E-10). Genomic features of interest are displayed on the x-axis. Black dotted lines indicate the boundaries of the *ter1* and *ter2* MatP domains. **(D)** Ratio plot of Δ*matP* (Δ*matP)* and *matP*$^+$ (WT) contact signals for each 5-kbp bin along ChrI and ChrII. A decrease or increase in contacts in Δ*matP* cells compared with *matP*$^+$ cells is represented with a blue or red colour, respectively. White indicates no differences between the two conditions. Genomic features of interest are indicated on the bottom and left axes. Black dotted lines indicate the boundaries of the *ter1* and *ter2* MatP domains.

Figure 2. MatP increases cohesion in the immediate vicinity of *dif1* and *dif2*.

(A) Top panel: relative longitudinal axis position of single spots. The new and old pole positions are set to 0 and 1, respectively. Results correspond to a median number of 2050 cells for each locus (Table S3A). Bottom panel: relative distance along the longitudinal axis between sister copies of each tagged locus in old cells. Results correspond to a median number of 1035 cells

752 for each locus (Table S3B). The median (disk), first and third quartile (horizontal marks) of the
753 positions/sister distances are shown for each tagged locus. Solid lines: expected position/sister
754 distance of intermediate loci; Dashed lines: the expected symmetrical position/sister distance
755 of loci on the left replication arm of ChrI; Blue and pink: ChrI; green and orange: ChrII; blue
756 and green: *matP*$^+$ cells (WT); pink and orange: Δ*matP* cells (Δ*matP*); Arrows: limits of the
757 regions where MatP influences the cellular positions of loci and sister spot distances. **(B)** Top
758 panel: spot duplication frequency (Table S3B). Grey dashed lines: expected decrease in spot
759 duplication frequency based on OI and R2I results, provided that sister chromatid cohesion is
760 constant along the genome. Grey bars: increase in duplication frequency of each locus in
761 Δ*matP* cells. Middle panel: Cre/*loxP*-based Hi-SC2 analysis of the relative frequency of
762 contacts of newly-replicated copies behind replication forks. Bottom panel: FtsK/XerCD/*dif1*-
763 based Hi-SC2 analysis of the relative frequency of contacts of sister copies during septum
764 closure. Results are shown at a 40 kbp resolution. Black dotted lines indicate the zones where
765 sister chromatid contacts are less frequent in Δ*matP* cells than in WT cells. Grey surfaces
766 highlight the global reduction of sister chromatid contacts in these zones. The corresponding
767 percentages of reduction is indicated.

768 **Figure 3. MatP increases cohesion in highly enriched *matS* regions.**

769 **(A)** MCH1 chromosome map. Regions originating from ChrI and ChrII are depicted in blue and
770 green, respectively. *ori1*, *dif2*, SI, VPI1, VPI2, VSP1, VSP2, O-antigene cluster, *crtS* and
771 positions of the loci tagged for microscopic observation are indicated as in Figure 1. **(B)** ChIP-
772 seq analysis of the binding of *V. cholerae* MatP in MCH1. Relative sequence enrichment profile
773 along MCH1 genome (100 bp sliding average). The profile was scaled between 0 (lowest
774 enrichment locus along the whole genome) and 1 (highest enrichment locus over the whole
775 genome, indicated with a star). Genomic features of interest are displayed on the x-axis. **(C)**
776 Top panel: relative longitudinal axis position of each tagged locus in young cells. Cells were
777 oriented using either *ori1* as in Figure 1C or *dif2* on the basis that it is located at the new pole
778 of newborn cells (Table S3A). Bottom panel: relative distance along the longitudinal axis of
779 sister copies of each tagged locus in old cells. Results correspond to a median number of 2116

780 cells for each locus (Table S3B). The median (disk), first and third quartile (horizontal marks)
781 of the positions/sister distances are shown for each tagged locus. Solid lines: expected
782 position/sister distance of intermediate loci; Dashed lines: the expected symmetrical
783 position/sister distance of loci on the left replication arm; Blue and pink: regions originating
784 from ChrI; green and orange: regions originating from ChrII; blue and green: *matP* $^{+}$ cells
785 (MCH1); pink and orange: Δ*matP* cells (MCH1 Δ*matP*); Arrows: limits of the regions where
786 MatP influences the cellular positions of loci and sister spot distances. **(D)** Top panel: spot
787 duplication frequency (Table S3B). Grey dashed lines: expected decrease in spot duplication
788 frequency based on OI, R1I and R2I results, provided that sister chromatid cohesion is
789 constant along the genome. Grey bars: increase in duplication frequency of each locus in
790 Δ*matP* cells. Middle panel: Cre/*loxP*-based Hi-SC2 analysis of the relative frequency of
791 contacts of newly-replicated copies behind replication forks. Bottom panel: FtsK/XerCD/*dif1*-
792 based Hi-SC2 analysis of the relative frequency of contacts of sister copies during septum
793 closure. Results are shown at a 40 kbp resolution. Black dotted lines indicate the zones where
794 sister chromatid contacts are less frequent in MCH1 Δ*matP* cells than in MCH1 cells. Grey
795 surfaces highlight the global reduction of sister chromatid contacts in these zones. The
796 corresponding percentage of reduction is indicated.

797 **Figure 4. MatP action depends on the number and local density of *matS* sites.**

798 **(A)** and **(F)** JVV024 and EPV487 chromosome maps, respectively. ChrI and ChrII are depicted
799 in blue and green, respectively. The position of the *matS* sites on JVV024 ChrI and ChrII are
800 indicated by pink and orange triangles, respectively. The two *matS* sites that were deleted from
801 JVV024 ChrI and inserted in its ChrII are depicted by white and pink triangles with a black
802 contour, respectively. The inverted region in EPV487 *ter1* is highlighted in red. Genomic
803 features of interest are indicated as in Figure 1C. **(B)** and **(G)** ChIP-seq analysis of the binding
804 of *V. cholerae* MatP in JVV024 and EPV487, respectively. The 100 bp (top panel) and 40 kbp
805 (bottom panel) sliding average profiles are shown to indicate the *matS* sites and to highlight
806 the enrichment of MatP in *ter1* and *ter2*. Genomic features of interest are indicated on the x-
807 axis as in Figure 1C. **(C)** and **(H)** FtsK/XerCD/*dif1*-based Hi-SC2 analysis of the relative

frequency of contacts of sister copies during septum closure in JVV024 and EPV487, respectively. Results are shown at a 40 kbp resolution. Genomic features of interest are indicated on the x-axis as in Figure 1C. **(D)** Cells were classified in four categories as a function of the number of DI and DII spots (1 DI & 1 DII spots, 2 DI &1 DII spots, 1 DI & 2 DII spots, and 2 DI & 2 DII spots). Left panel: frequency of cells from each category; Middle panel: frequency of cells from the second category over the number of cells from the second and third categories; Right panel: zoom on the frequency of cells from the fourth category. Results correspond to at least 2584 analysed cells (Table S3C). ** The difference is statistically different (chi2 test; $p < 0.001$); n.s., the difference is not statistically significant (chi2 test; $p > 0.5$). **(E)** Distance along the longitudinal axis between sister copies of DI and DII spots. The median (horizontal bar), the 25th and the 75th percentiles (open box) and the 5th and the 95th percentiles (error bars) of the sister spot distances are represented for each sample. Results correspond to at least 248 cells for each locus (Table S3). The distances between sister DI spots of N16961, EPV487 and JVV024 cells were significantly different (Wilcoxon-Mann-Whitney test, p-value<0.01). The distances between sister DII spots of N16961 and EPV487 cells were significantly different (p-value <0.01) but not those of N16961 and JJV024 cells.

Figure 5. MatP acts independently of cell division.

(A) Cell cycle choreography of the DI locus in WT and mutant *V. cholerae* strains. Each panel shows the compilation of individual cell cycle traces (WT: 81; Δ*matP*: 62; *matP* Δdimer: 85; *matP* Δtetra: 69; Δ*zapA*: 48; Δ*zapB*: 85). In the heat maps, black corresponds to the lowest and dark red to the highest intensities. y-axis: position along the cell length, with 0 corresponding to the new pole and 1 to the old pole. x-axis: % of the cell cycle, with 0 corresponding to birth and 100 to scission. **(B)** Relative distance between sister copies of the DI (blue) and DII (green) locus. The median (horizontal bar), the 25th and the 75th percentiles (open box) and the 5th and the 95th percentiles (error bars) of the sister spot distances are represented for each sample. Dotted lines highlight the median DI (blue) and DII (green) sister spot distance in WT cells. The distance between sister DI and DII spots of Δ*matP* and *matP* Δdimer cells were significantly different from those of N16961 cells (Wilcoxon-Mann-Whitney

test, p-value<0.01) and were not different between each other. The distances between sister DI spots of *matP* Δtetra, Δ*zapA* and Δ*zapB* cells were significantly different from those of N16961 cells (p-value<0.01). (**C)** Cellular localisation of DI foci over-time in time lapse experiments in *ftsZ84*^{ts} (top panel) and *ftsZ84*^{ts} Δ*matP* (bottom panel) cells grown at 42°C. One frame was taken every 3 minutes. On the top-right corner of each frame is indicated the time in minutes from the beginning of imaging. Scale bar = 2 µm.

SUPPLEMENTARY FIGURES LEGENDS

Figure S1. MatP creates a macrodomain in the *ter1* and *ter2* chromosomal zones.

(A) Relative enrichment of ChIP-seq reads at 4 locations harbouring an identical *matS* motif. The locations are identified based on the replicon they belong to and their position on this replicon. The first three locations were identified in the ChIP-seq analysis as MatP binding sites. The 4th position was identified with MCAST using the MEME *matS* consensus. Note the different levels of sequence enrichments on the first three sites and the absence of enrichment on the 4th site. **(B)** Consensus sequence of *V. cholerae* MatP binding, built using the Meme suite based on the ChIP-seq sequences. **(C)** 40 kbp sliding average profile of the number of *matS* sites along ChrI and ChrII indicating the expected enrichment of MatP-bound sequences at the centre of *ter1* and *ter2* induced by the local density of *matS* sites. **(D)** 40 kbp sliding average profile of the ChIP-seq data from Figure 1C, showing the actual enrichment of MatP at the centre of *ter1* and *ter2*. **(E)** and **(F)** Normalized contact map obtained from asynchronous populations (minimal medium, 5 kbp resolution) of WT and Δ*matP V. cholerae* cells, as indicated. The colour scale reflects the frequency of contacts between two regions of the genome, from white (rare contacts) to dark purple (frequent contacts). Genomic features of interest are indicated on the bottom and left axes. Black dotted lines indicate the boundaries of the *ter1* and *ter2* MatP domains. Genomic features of interest are indicated on the x-axis as in Figure 1C.

Figure S2. MatP increases cohesion in the immediate vicinity of *dif1* and *dif2*.

(A) Relative longitudinal axis position of each tagged locus in old cells. Results correspond to a median number of at least 210 cells for each locus. Cells were oriented on the basis that *ori1* is located at the old pole of newborn cells and that one of its replicated copies remains at the old pole during the replication/segregation cycle. By convention, the longitudinal axis coordinates of the new pole and the old pole are set to 0 and 1, respectively. The median (disk), first and third quartile (horizontal marks) of the positions/sister distances are shown. Solid lines: expected position/sister distance of intermediate loci; Dashed lines: the expected symmetrical position/sister distance of loci on the left replication arm of ChrI; Blue and pink: ChrI; green and orange: ChrII; blue and green: *matP*$^{+}$ cells (WT); pink and orange: Δ*matP* cells (Δ*matP*). **(B)** Comparison of FtsK/XerCD-mediated recombination of short and long *dif1* cassettes, indicative of inter and intra-molecular events, respectively. Results are shown at a 40 kbp resolution.

Figure S3. MatP increases cohesion in highly enriched *matS* regions.

(A) 40 kbp sliding average of the MatP ChIP-seq data from MCH1. Blue and green lines: relative sequence enrichment profiles along the DNA originating from ChrI and ChrII, respectively. The profiles were scaled between 0 (lowest enrichment locus along the whole genome) and 1 (highest enrichment locus, indicated by a star). Genomic features of interest are displayed on the x-axis. **(B)** Relative longitudinal axis position of each tagged locus in young cells. Results correspond to a median number of at least 134 cells for each locus. Cells were oriented using OI or DII (as described in Figure 1C and Figure 3C). By convention, the longitudinal axis coordinates of the new pole and the old pole are set to 0 and 1, respectively. The median (disk), first and third quartile (horizontal marks) of the positions/sister distances are shown. Solid lines: expected position/sister distance of intermediate loci; Dashed lines: the expected symmetrical position/sister distance of loci on the left replication arm of the MCH1 chromosomes; Blue and pink: regions originating from ChrI; green and orange: regions originating from ChrII.

Figure S4. MatP action depends on the number and local density of *matS* sites.

(A) FtsK/XerCD/*dif1*-based Hi-SC2 analysis of the relative frequency of contacts of sister copies during septum closure in EPV487 Δ*matP* cells. Results are shown at a 40 kbp resolution. ChrI and ChrII results are shown in blue and green, respectively. Results in the inverted zone of ChrI are highlighted in red. Solid black line: sister contact frequencies along the genome of EPV487 *matP*$^{+}$ cells from Figure 4C. **(B)** Frequency of cells with separated DI and DII sister copies as a function of cell length. Blue, red and pink: frequency of separated DI spots in WT, EPV487 and JVV024 cells, respectively; Green, black, orange: frequency of separated DII spots in WT, EPV487 and JVV024 cells, respectively.

Figure S5. MatP acts independently of cell division.

(A) Examples of the DI locus time-lapse individual cell cycles in *V. cholerae* WT (top panels) and Δ*matP* (bottom panels) cells. **(B)** Cell cycle choreography of the OI locus in WT *V. cholerae* cells (compilation of 50 individual cell cycles) and Δ*matP* (compilation of 34 individual cell cycles). **(C)** Examples of the OI locus time-lapse individual lineages in *V. cholerae* WT (top panels) and Δ*matP* (bottom panels) cells. In the heat maps, black corresponds to the lowest and dark red to the highest intensities. y-axis: position along the cell length, with 0 corresponding to the new pole and 1 to the old pole (ABC). **(D)** 100 bp (left panels) and 40 kbp (right panels) sliding average of the MatP ChIP-seq data from *matP* Δtetra (top panel), *ftsZ84*^{ts} grown at 30°C (middle panel) and *ftsZ84*^{ts} grown at 42°C (bottom panel) *V. cholerae* cells. Blue/Pink and Green/Orange lines: relative sequence enrichment profiles along ChrI and ChrII, respectively. The profiles were scaled between 0 (lowest enrichment locus along the whole genome) and 1 (highest enrichment locus along the whole genome). Genomic features of interest are displayed on the x-axis.

SUPPLEMENTARY TABLES AND FILE LEGENDS

Table S1. MatP-bound N16961 *V. cholerae matS* sites. The table indicates the location of the central base of each site, its sequence and the sequence of 10 bp on its left (L) and right (R) side. Stars indicate sites present in repeated regions. The Meme P_value indicates how well each site matches the MEME weight matrix. The Mcast score indicates the similarity of the sequence to the MEME motif. A hyphen indicates sites that were not identified with Mcast. Sites falling within the MatP domains of ChrI and ChrII are highlighted in bold.

Table S2. N16961 *V. cholerae matS* sites not bound by MatP. The sites were identified using MCAST. *: MCAST-identified site with the same sequence as the *matS* site identified by ChIP-seq at the 1903191 ChrI position; **: MCAST-identified site with the same sequence as the *matS* sites identified by ChIP-seq at the 481992 ChrI and 471499 and 522018 ChrII positions. The ChIP-seq profile of these 4 sites is shown in Figure S1A. Sites falling within the MatP domains of ChrI and ChrII are highlighted in bold.

Table S3. Number of cells analysed in fluorescence microscopy snapshots. (A) Number of oriented N16961, N16961 Δ*matP*, MCH1 and MCH1 Δ*matP* cells used in Figure 2A and S2A. N16961 cells were oriented using the positions of the OI spots. MCH1 cells were oriented using the positions of the OI spots or the DII spots **(B)** Number of 1-spot and 2-spots N16961, N16961 Δ*matP*, MCH1 and MCH1 Δ*matP* cells used in Figure 2B and 3D. **(C)** Number of 1-spot and 2-spots in N16961, JJV024 and EPV487 cells harbouring a tag at DI and DII used in Figure 4D, and total number of cells showing fluorescence at both DI and DII used in Figure 4E.

Table S4. Distribution of MatP-bound *matS* sites in MCH1. The table indicates the location of the central base of each site, its sequence and the sequence of 10 bp on its left (L) and right (R) side. Sites falling within the MatP domains of ChrI and ChrII are highlighted in bold.

Table S5. Distribution of MatP-bound *matS* sites in JJV024. The table indicates the location of the central base of each site, its sequence and the sequence of 10 bp on its left (L) and right (R) side. Stars indicate sites present in repeated regions. Sites falling within the MatP domains

of ChrI and ChrII are highlighted in bold. The two sites that were moved from ChrI to ChrII are indicated in pink.

Table S6. Distribution of MatP-bound *matS* sites in EPV487. The table indicates the location of the central base of each site, its sequence and the sequence of 10 bp on its left (L) and right (R) side. Stars indicate sites present in repeated regions. Sites falling within the MatP domains of ChrI and ChrII are highlighted in bold. The sites within the inverted region or ChrI are highlighted in red.

Table S7. List of bacterial strains, plasmids and oligonucleotides used in this study.

File S1. Detailed description of bacterial strains construction.

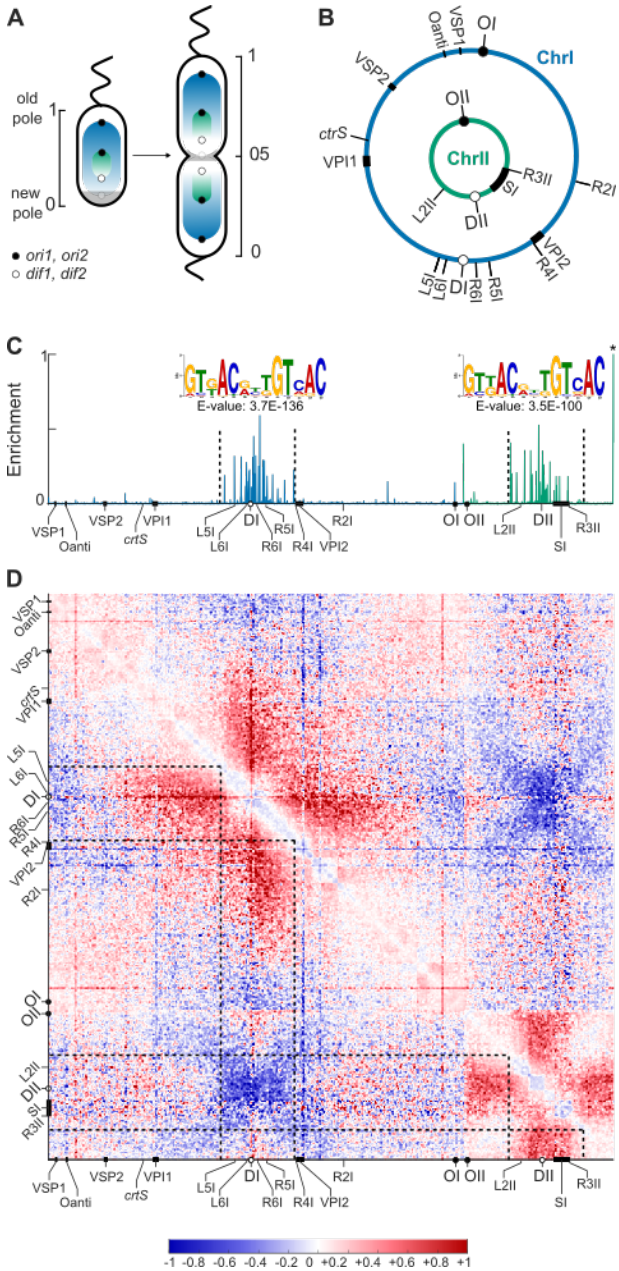
A
old pole
new pole
1
0
1
05
0
● ori1, ori2
○ dif1, dif2
B
ChrI
ChrII
OI
OII
DI
DII
VSP1
Oanti
VSP2
ctrS
VPI1
R3II
SI
R2I
L2II
VPI2
R4I
L5I
L6I
R6I
R5I
C
Enrichment
E-value: 3.7E-136
E-value: 3.5E-100
VSP1
Oanti
VSP2
VPI1
crtS
L5I
L6I
DI
R6I
R5I
R4I
VPI2
R2I
OI
OII
L2II
DII
SI
R3II
D
-1 -0.8 -0.6 -0.4 -0.2 0 +0.2 +0.4 +0.6 +0.8 +1

Figure 1

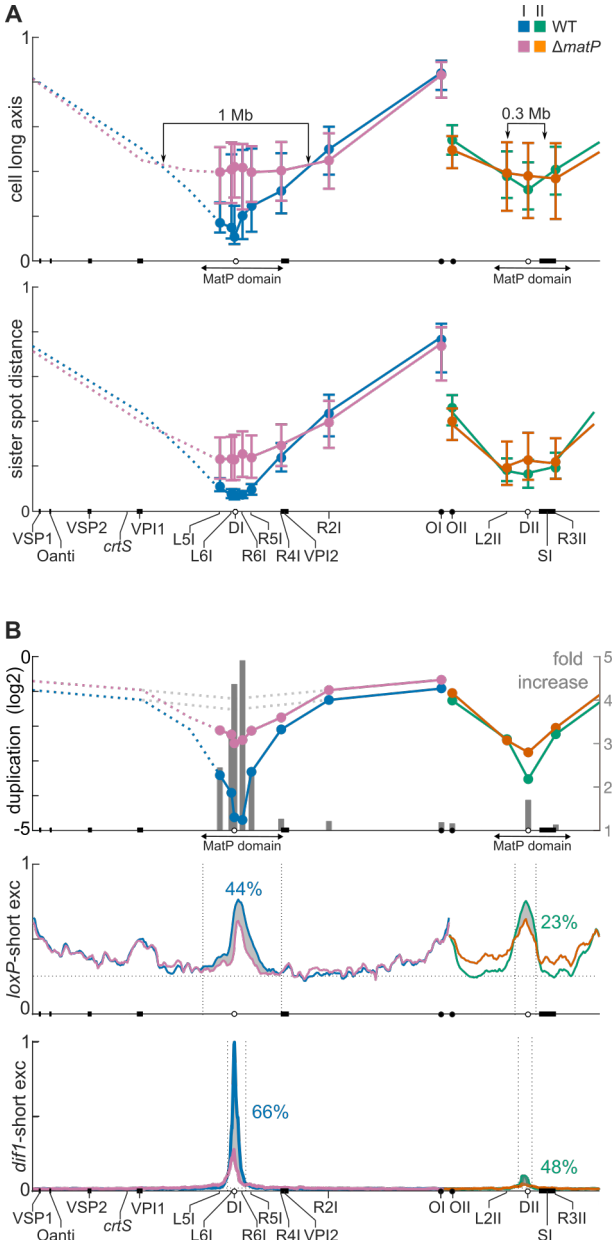
A
I II
WT
ΔmatP
cell long axis
1 Mb
0.3 Mb
MatP domain
MatP domain
sister spot distance
VSP1
Oanti
VSP2
crtS
VPI1
L5I
L6I
DI
R6I
R5I
R4I
VPI2
R2I
OI OII
L2II
DII
SI
R3II
B
duplication (log2)
fold increase
loxP-short exc
44%
23%
dif1-short exc
66%
48%

Figure 2

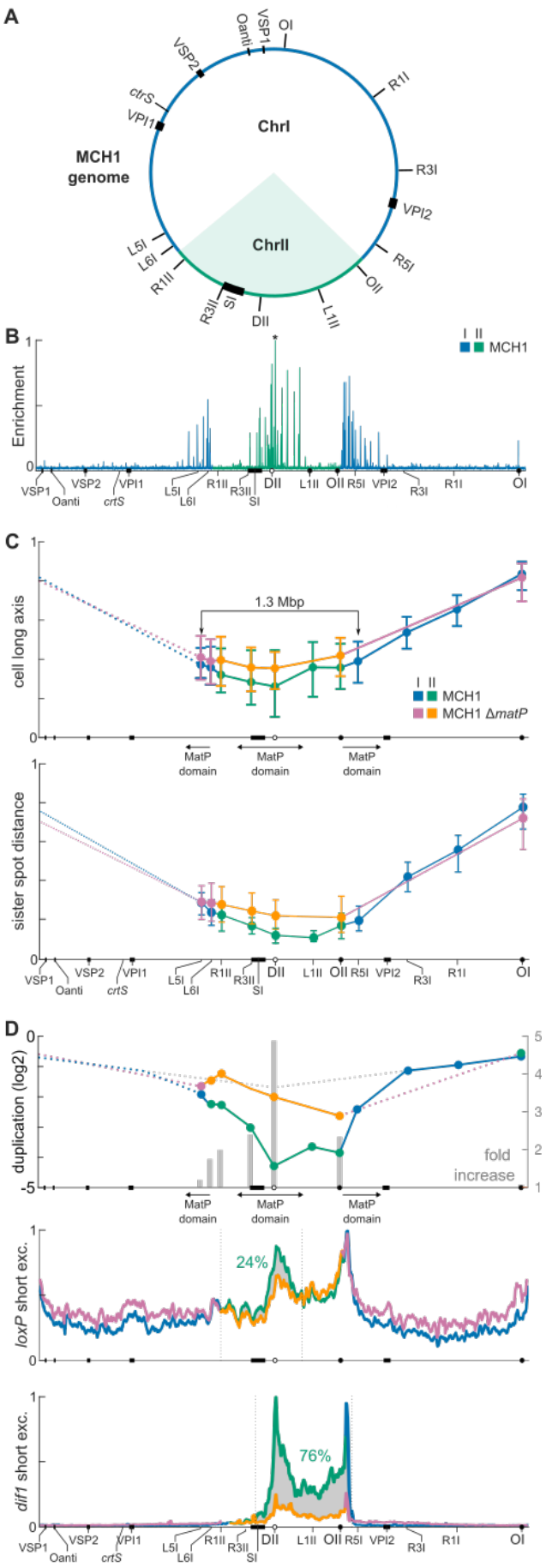
A
MCH1
genome
ChrI
ChrII
OI
VSP1
Oanti
VSP2
ctrS
VPI1
R1I
R3I
VPI2
R5I
OII
L1II
DII
SI
R3II
R1II
L6I
L5I
B
Enrichment
I II
MCH1
C
cell long axis
1.3 Mbp
MCH1
MCH1 ΔmatP
MatP
domain
sister spot distance
D
duplication (log2)
fold
increase
loxP short exc.
24%
dif1 short exc.
76%

Figure 3

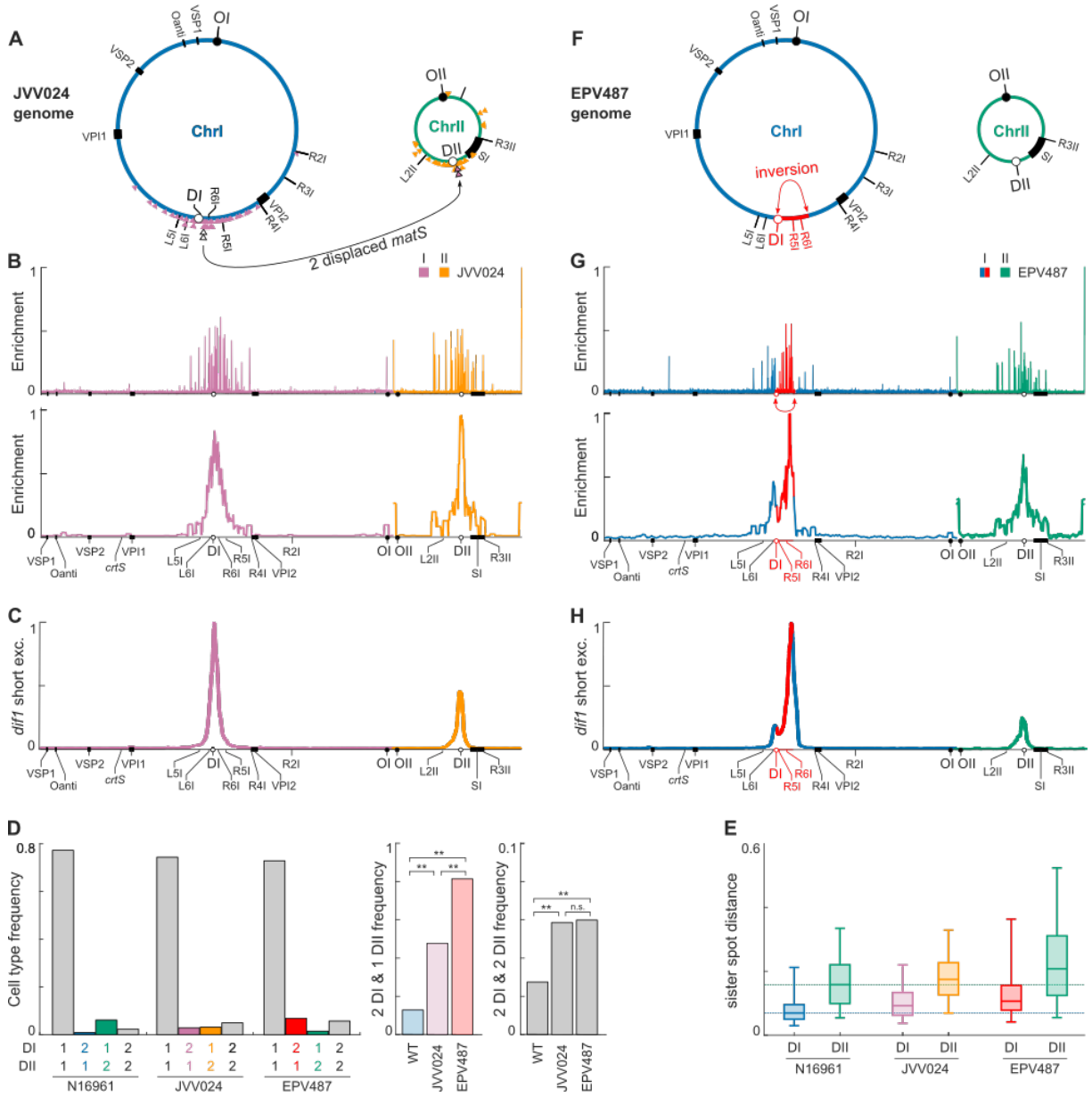
A
JVV024 genome
ChrI
ChrII
2 displaced matS
B
JVV024
Enrichment
C
dif1 short exc.
D
Cell type frequency
N16961
JVV024
EPV487
2 DI & 1 DII frequency
2 DI & 2 DII frequency
WT
n.s.
E
sister spot distance
F
EPV487 genome
inversion
G
H

Figure 4

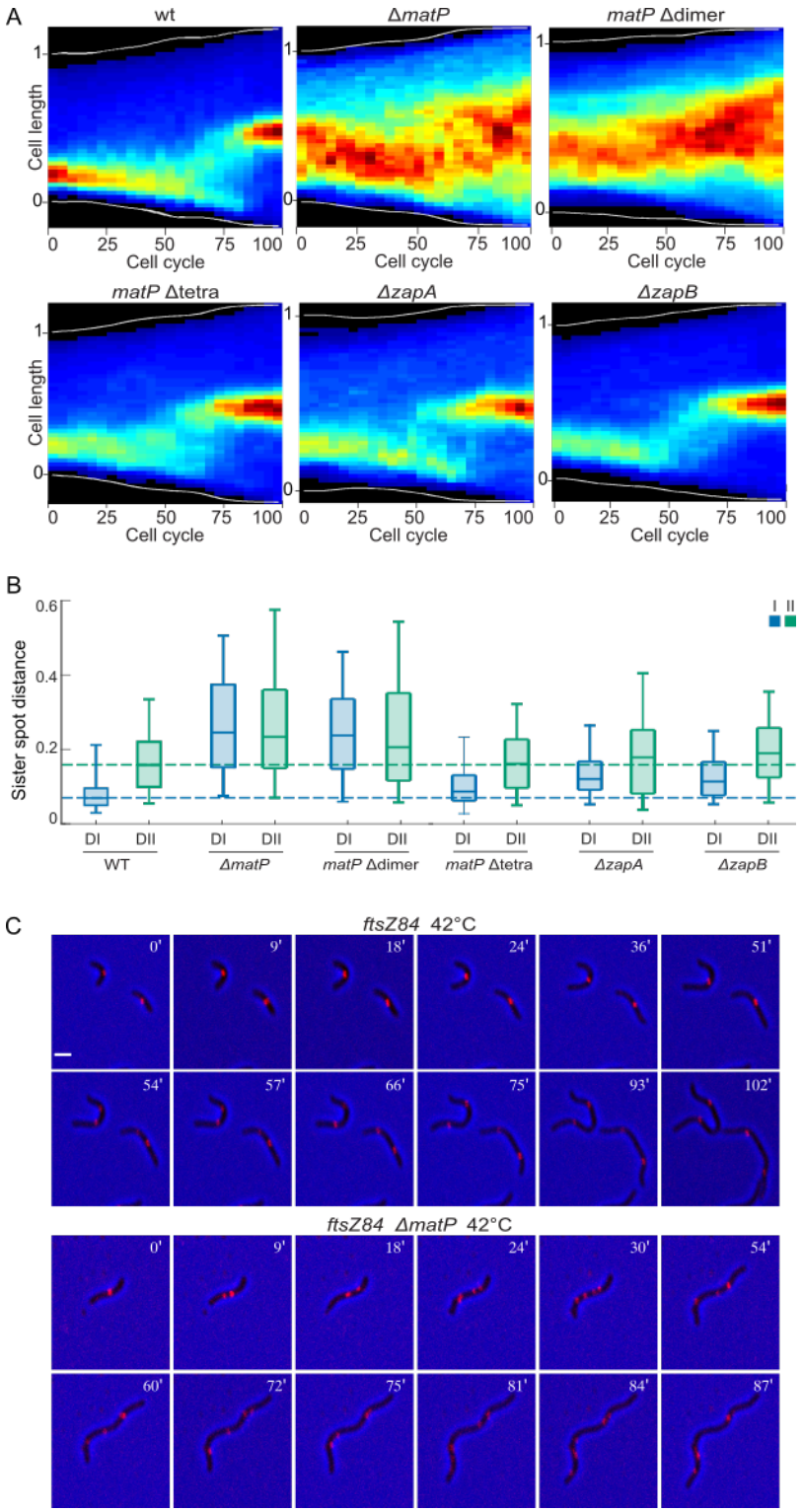
A
wt
ΔmatP
matP Δdimer
matP Δtetra
ΔzapA
ΔzapB
Cell length
Cell cycle
B
Sister spot distance
I II
DI DII
WT
ΔmatP
matP Δdimer
matP Δtetra
ΔzapA
ΔzapB
C
ftsZ84 42°C
ftsZ84 ΔmatP 42°C

Figure 5